THE JOURNAL OF PHYSICAL CHEMISTRY C
A JOURNAL OF THE AMERICAN CHEMICAL SOCIETY

pubs.acs.org/JPCC

Article

Long-Range Ionic and Short-Range Hydration Effects Govern Strongly Anisotropic Clay Nanoparticle Interactions

Andrea Zen,*,○ Tai Bui,○ Tran Thi Bao Le, Weparn J. Tay, Kuhan Chellappah, Ian R. Collins, Richard D. Rickman, Alberto Striolo, and Angelos Michaelides*

Cite This: https://doi.org/10.1021/acs.jpcc.2c01306

Read Online

ACCESS | Metrics & More | Article Recommendations | Supporting Information

ABSTRACT: The aggregation of clay particles in aqueous solution is a ubiquitous everyday process of broad environmental and technological importance. However, it is poorly understood at the all-important atomistic level since it depends on a complex and dynamic interplay of solvent-mediated electrostatic, hydrogen bonding, and dispersion interactions. With this in mind, we have performed an extensive set of classical molecular dynamics simulations (included enhanced sampling simulations) on the interactions between model kaolinite nanoparticles in pure and salty water. Our simulations reveal highly anisotropic behavior, in which the interaction between the nanoparticles varies from attractive to repulsive depending on the relative orientation of the nanoparticles. Detailed analysis reveals that at large separation (>1.5 nm), this interaction is dominated by electrostatic effects, whereas at smaller separations, the nature of the water hydration structure becomes critical. This study highlights an incredible richness in how clay nanoparticles interact, which should be accounted for in, for example, coarse-grained models of clay nanoparticle aggregation.

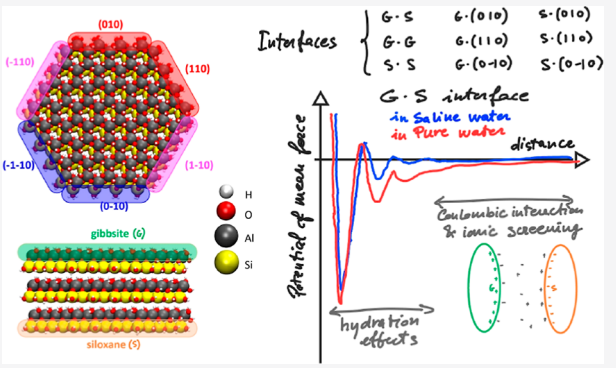

INTRODUCTION

Clay particles are all around us: present in the Earth's crust, soil, the ocean floor, and the atmosphere as aerosols. Clays have been extensively used since antiquity in pottery, as building and writing materials, and more. Clays are also critical to contemporary challenges: for example, as atmospheric ice nucleating agents, they are relevant to climate change; the ability of clays to trap toxic (including nuclear) waste is important for environmental remediation; and as porous materials, they filter and dictate the flow of water and other fluids through rocks.[1]

Understanding the aggregation of individual clay particles into larger agglomerates is critical to explaining and controlling the behavior of clays in many of the above examples. However, at the atomic scale, clay particle agglomeration is poorly understood. Partly, this is down to the challenge of characterizing and tracking the agglomeration of clay particles in solution but also because of the wealth of variables that are inevitably relevant to the agglomeration process. Parameters such as particle size, shape, chemical composition, temperature, pressure, and solvent effects will all play a role.[2] A further challenge is the inherent chemical complexity of clay particles: as (alumino)-silicate clays interact through a complex interplay of electrostatic, hydrogen bonding, and van der Waals (vdW) dispersion forces; with all these interactions mediated by the aqueous electrolyte solution separating individual particles.[3]

The inherent (and interesting) complexity of clay particle aggregation has motivated a large body of experimental[4−14] and computational[15−37] work aimed at understanding clay particle association under well-defined conditions, as well as related questions about the structure and dynamics of the water−clay interface. Being the simplest, one of the most abundant, and also one of the most technologically relevant clays, kaolinite ($Al_2(OH)_4Si_2O_5$), has emerged as a widely studied model system. Indeed, kaolinite can now essentially be considered the "fruit fly" system of physical chemistry/chemical physics research on clay particles. However, the nature of kaolinite nanoparticle association under even simple and well-defined conditions is still not understood. This is what we aim to address in the current study through a systematic set of computational studies, aiming specifically to understand the following questions: (i) are the interactions between clay (nano)-particles in solution attractive or repulsive?; (ii) does the nature of the interaction depend on the facets of the (nano)-particles that interact and if so to what

Received: February 23, 2022
Revised: April 14, 2022

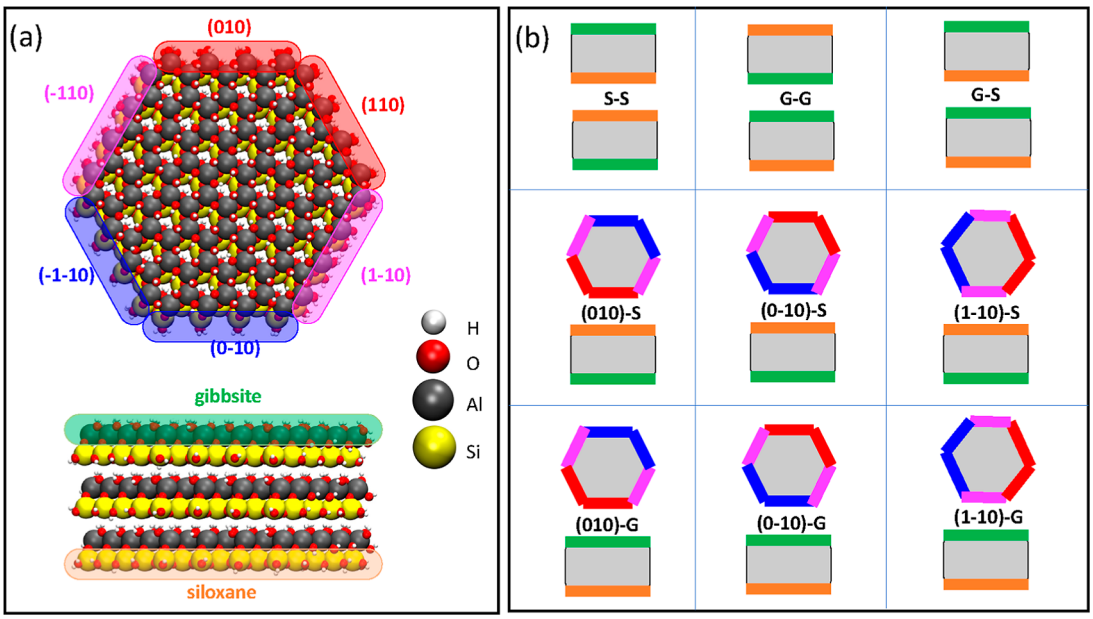

Figure 1. Overview of the model kaolinite nanoparticles considered in this study. (a) Representation of two kaolinite particles in the edge-to-face orientation. The six edges (top) are called after their Miller indices of the crystallographic structure,[39] and the two inequivalent basal surfaces (bottom), (001) and (00−1), are called gibbsite (G) and siloxane (S) faces, respectively, according to the literature. White, red, gray, and yellow spheres represent the hydrogen, oxygen, aluminum, and silicon atomic species, respectively. We emphasize the five nonequivalent surfaces (the six edges are 2-by-2 equivalent) using different colors. (b) Nine representative orientations of two kaolinite particles considered in this work.

extent?; (iii) what role does the aqueous solution play in the association process?; and (iv) what are the length scale(s) of the particle−particle interactions?

To answer these questions and to gain a better understanding of the factors that influence kaolinite particle agglomeration in aqueous solutions, we used molecular dynamics simulations to explore the association of clay nanoparticles. Since kaolinite nanoparticles most often occur as hexagonal platelets,[38] we modeled the association of hexagonal clay nano-platelets. Figure 1a shows representation of the simulated nanoparticles. In order to capture the role the (dynamic) solvent molecules play in the association process, we computed potential of mean force (PMF) curves between two kaolinite particles with varying orientations, see Figure 1b, in both pure and saline water environments. The contributions of interparticle interactions are disentangled into the vdW and Coulombic potentials. The effect of the hydration films on the PMF profiles is then investigated, with a particular emphasis on the structural and dynamical properties of water molecules confined between the two approaching surfaces. As the presence/absence of ions in solution affects differently the different contributions determining the overall interparticle interactions, we are able to elucidate the effects of salt on the evaluated PMFs.

■ COMPUTATIONAL METHODS

The MD simulations employing force field potentials have all been performed using the LAMMPS package.[40] In each simulation cell, there are two kaolinite nanoparticles and 10,000 to 11,000 water molecules. An image of the nanoparticles in the edge-to-face configuration—but without any water present—is shown in Figure 1a. An image of the full simulation cell including the water molecules is shown in Figure S1 of Supporting Information. The kaolinite nanoparticles are prepared, as described in Section S1 of Supporting Information. To simulate the saline solution, sodium chloride ions corresponding to the salinity of 1.2 M were added to the system. In line with ref 17, the simulation cell is roughly 60 × 60 × 100 Å^3. A simulation box of this size is sufficiently large to avoid finite size effects, as evidenced by: (i) the density of water, see Figures 3c and S10g−i of Supporting Information; and (ii) the diffusion coefficient of water, see Figure S13 of Supporting Information, in the region between the two kaolinite particles, both of which reach the bulk value. In the face-to-face orientation both the nanoparticles have the basal faces parallel to the *xy*-plane, whereas in the face-to-edge orientation, one nanoparticle (the lower in our setups) has the basal faces parallel to the *xy*-plane, and the other nanoparticle has the basal faces orthogonal to the *xy*-plane, and it is placed above the first nanoparticle.

Force Fields. The simulations employed the ClayFF potential[37,41−43] for kaolinite and the rigid SPC/E model[44] for water. The sodium, Na^+, and chloride ions, Cl^-, were modeled as a single charged Lennard-Jones sphere with parameters taken from the study of Smith and Dang without polarizability.[45] Interactions between unlike atom types were calculated using the standard Lorentz−Berthelot mixing rules. The SHAKE algorithm[46] is used to constrain the rigid water molecule and the OH distance in the hydroxyl groups of kaolinite. Additional constraints on the kaolinite atoms have been added to enhance the stability of the nanoparticles, following previous work.[47,48] Real-space interactions were truncated at 10 Å with corrections to the energy applied, and a particle−particle−particle−mesh solver was used to account for long-range electrostatics.[49] The integration step in the MD simulations is 1 fs. We tested the above setup on the adsorption of a single water molecule of the Na^+ cation and Cl^- anion on the siloxane and gibbsite faces, and we registered reasonable agreement with benchmark *ab initio* evaluations (see Section S2 and Table S1 in Supporting Information), in agreement with other studies from the literature.[35,37,50]

https://doi.org/10.1021/acs.jpcc.2c01306
J. Phys. Chem. C XXXX, XXX, XXX−XXX

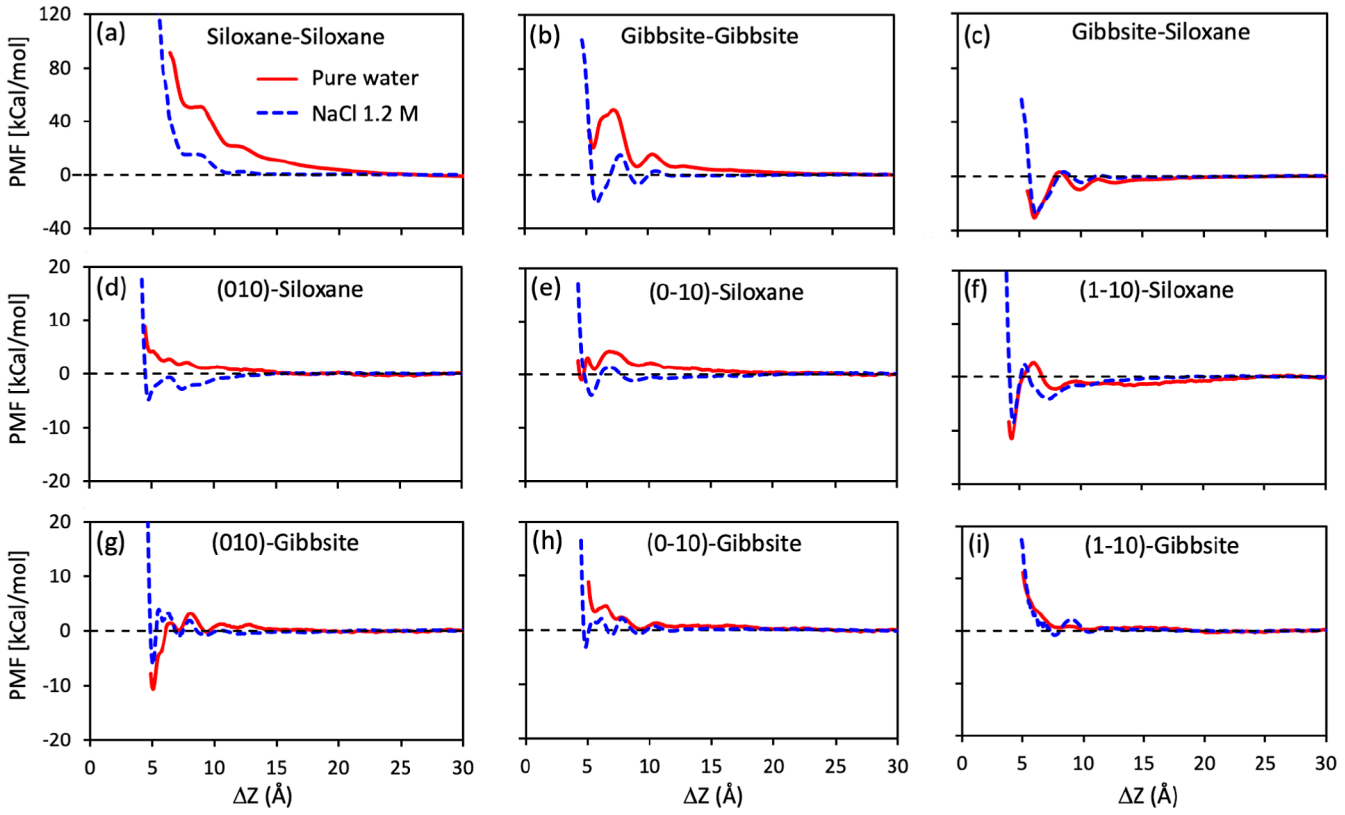

Figure 2. Interaction between two kaolinite nanoparticles at different orientations. (a–c) for face-to-face interfaces; (d–i) for edge-to-face interfaces. Red and blue curves are the PMF profiles in pure water and in 1.2 M of sodium chloride solution, respectively. They are obtained from US simulations in the *NVT* ensemble at a temperature of 350 K, employing the ClayFF atomic force field for the kaolinite particles and the SPC/E water model. The abscissa, ΔZ, is the minimum distance among the "heavy" atoms (i.e., Al or Si atomic species) of the two nanoparticles.

Simulation Protocol. To simulate the system at the desired temperature and pressure, an equilibrium simulation at a pressure of 200 bar and temperature of 350 K was initially conducted for 1 ns in the *NPT* ensemble [constant number (N) of atoms/particles, pressure (P), and temperature (T)]. Moreover, the system associated to each specific orientation has been equilibrated in the *NVT* ensemble [constant number of atoms/particles, volume (V), and temperature] at 350 K for over 1 ns by applying separate Nosé-Hoover chain thermostats[51] to water and nanoparticles.

The umbrella sampling (US) technique[52,53] was employed to evaluate the PMF among two nanoparticles using the collective variable modules[54] implemented in LAMMPS.[40] The computational details for the US simulations are reported in the Supporting Information. In these simulations, a harmonic potential with a force constant of 10 kcal/(mol·m^2) or 50 kcal/(mol·m^2) is used to keep the upper particle at a specific distance from the bottom one to ensure good sampling overlap between adjacent sampling windows. In both the face-to-face and face-to-edge orientations, the lower nanoparticle is neither allowed to diffuse nor to rotate, with its heavy atoms (Al and Si) tethered to their initial position (using the fix spring/self-command in LAMMPS). The upper nanoparticle is allowed to translate but not to rotate (heavy atoms are constrained using the fix rigid command). The only exception is for the cases of the edge-to-face orientations, where a short simulation (around 100 ps, prior to imposing the rotational constraints) was performed to allow the upper particle to freely rotate and translate so that the edge of the top particle can preferentially interact with the basal surface of the bottom one. Consequently, the angle formed by the two particles are not precisely 90° afterward (the deviation is less than 10°). Note that the PMF is a function of the distance among the nanoparticles. There are several different ways to quantify this distance (see, for instance, Figure S1 in Supporting Information). The US constraint uses the distance among the centers of mass of the heavy atoms (i.e., Al and Si) of the two nanoparticles as it is easily computed in runtime during an MD simulation. In the Results and Discussion section, we report the results as a function of the minimum distance ΔZ among the heavy atoms of the two nanoparticles, which provides a direct indication of the thickness of the interface and facilitates the comparison among PMF curves relative to different orientations. We note that the procedure described above was followed for each orientation of the nanoparticles, as shown in Figure 1, panel (b) and discussed in the Results and Discussion section.

As noted above, the simulations reported in this work have been performed at 350 K, representing a typical temperature for inner earth oil reservoirs. We also performed additional simulations at 450 K on the gibbsite–siloxane orientation (see Section S4 and Figure S5 in Supporting Information). The effect of temperature on the PMF profile yields a minimal impact. This observation is in agreement with the observations of Ho and Criscenti.[17] Finally, it is important that the US MD simulations are long enough to sample properly the phase space. We performed some preliminary calculations, which indicated that a reasonable level of convergence in the PMF is already achieved when each US MD simulation is 3 ns long or more, see Figure S4 of Supporting Information. In our

https://doi.org/10.1021/acs.jpcc.2c01306
J. Phys. Chem. C XXXX, XXX, XXX−XXX

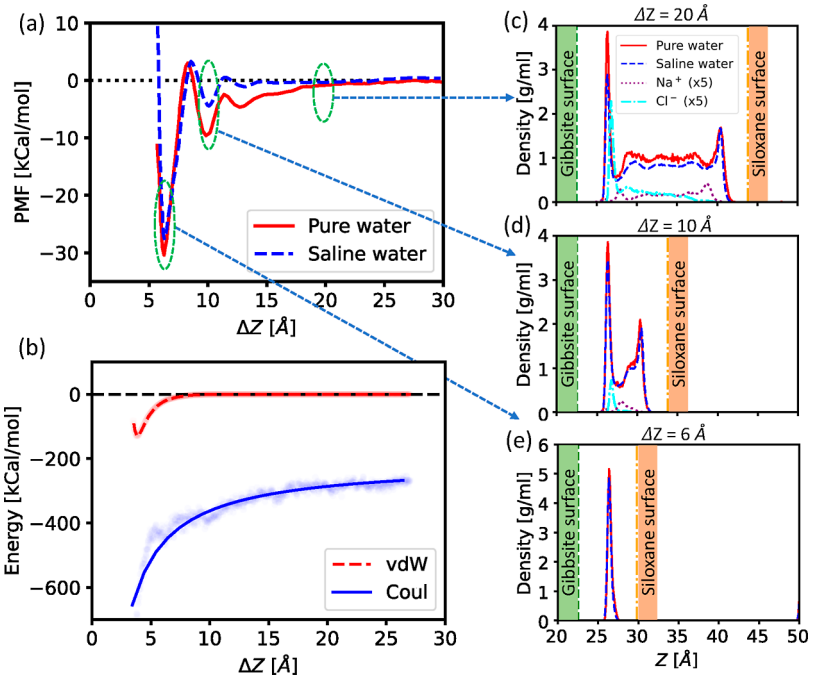

Figure 3. Overview of the interaction and the hydration for interfaces of different thicknesses. (a) PMF profiles between two kaolinite particles in pure and saline water systems for the gibbsite−siloxane orientation. (b) Decomposition of particle−particle interactions: vdW and Coulombic potentials as a function of the distance between the two particles. (c−e) Density profiles of water, Na^+, and Cl^- along the *Z*-direction of the simulation box calculated for the pure and saline water systems at the particle−particle distance of 20, 10, and 6 Å, respectively.

production calculations, we used at least 5 ns long US simulations.

RESULTS AND DISCUSSION

In the following sections, we first show and discuss the PMFs between kaolinite nanoparticles at different orientations, followed by an analysis of the energetic contributions of the free energy and how it determines the attractive or repulsive nature of the interaction between nanoparticles. We consider the structure of water and ions at the interface and elucidate how they determine the qualitative features of the PMF profile for narrow separation distances. Finally, we discuss the diffusion of kaolinite particles in solution.

Orientation Dependence of PMF Profiles. A hexagonal kaolinite platelet has eight interfaces with water: two inequivalent basal faces and six edges. A careful analysis of the six edges shows that some of them are indeed very similar, and we can identify only three inequivalent edges.[37,55] In particular, the (0 1 0) edge is roughly equivalent to the (1 1 0), the (0 −1 0) edge is roughly equivalent to the (−1 −1 0) surface, and the (1 −1 0) edge is roughly equivalent to the (−1 1 0) surface, see Figure 1. Thus, we limit our investigation to only one representative edge for each equivalent class. This leads to three representative edges: (0 1 0), (1 −1 0), and (0 −1 0). Therefore, in aqueous solutions, we evaluated nine distinct PMFs for particle−particle interactions, three of which are face-to-face oriented and six of which are edge-to-edge oriented. In real systems, we expect the presence of a variety of ions in water, either directly desorbed from rock surfaces or in the form of mineral salts. In addition, given that the kaolinite basal surface is polar,[56] ions in solution are likely to adsorb at the interface to compensate for the dipoles present within the nanoparticle.[30] To account for these issues, we performed simulations in both pure water and in the more realistic situation of saline water, with a 1.2 M sodium chloride (NaCl) concentration.

The PMF curves obtained from our simulations are shown in Figure 2. We find that the PMF profiles are highly dependent on the relative orientation between the two particles. In particular, the gibbsite−siloxane orientation is the most attractive, whereas the gibbsite−gibbsite and siloxane−siloxane orientations are overall repulsive. This behavior is explained qualitatively, at least for the pure water case, in terms of electrostatics, as a kaolinite nanoparticle forms a dipole with the siloxane surface negatively charged and the gibbsite surface positively charged. The face-to-edge orientations exhibited a highly variable pattern of behavior, with two out of six orientations being weakly attractive and the remaining being overall repulsive. The face-to-edge PMFs are noticeably flatter than the face-to-face PMFs. This is only in part explained by the size of the interface: in our simulations, the face-to-face orientation has an interface that is roughly 2.3 times larger than the face-to-edge, while the free-energy barriers in the former are much larger than a factor 2.3; see the plot of the PMF per surface area reported in Figure S6 of Supporting Information. It is likely that the atomically rough morphology of the edges prevents the formation of highly pronounced hydration layers, as observed in simulations conducted for hydrated crystalline versus amorphous silica, which could reduce the intensity of the resultant PMF profiles.[57−59]

The presence of ions in solution shows a significant impact on PMF profiles. Ions screen the long-range electrostatic interaction between the two particles, especially in the face-to-face oriented interfaces. In particular, siloxane−siloxane and gibbsite−gibbsite orientations exhibit decreased repulsion at large distances when ions are in solution. The greatest effect is observed on the interactions between the particles along the

https://doi.org/10.1021/acs.jpcc.2c01306
J. Phys. Chem. C XXXX, XXX, XXX−XXX

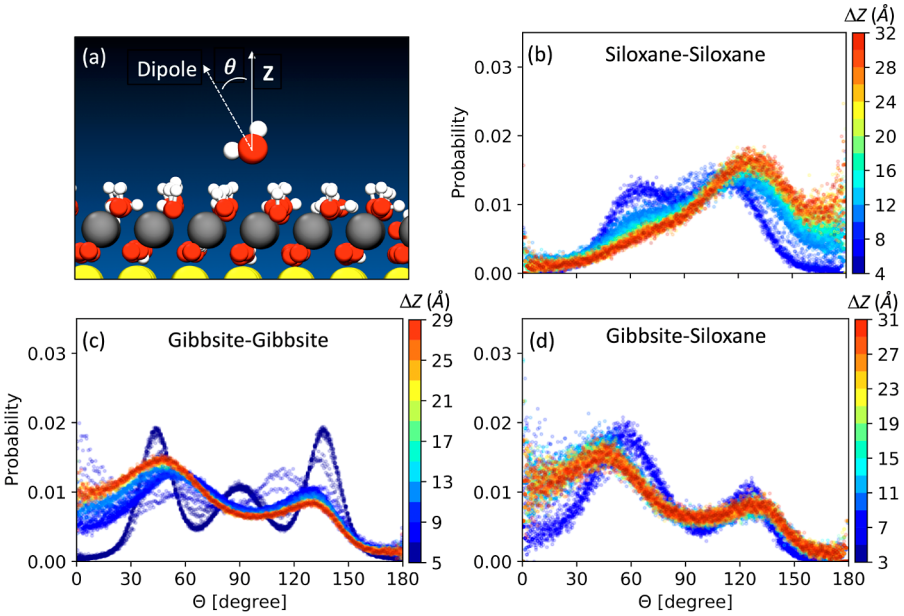

Figure 4. Orientation of water molecules at the interface. (a) Definition of the angle formed between water dipole moments and the *Z*-direction of the simulation box. (b–d) Distribution of the angle formed between the dipole vector of water molecules in the first hydration layer and the *Z*-direction of the simulation box. Color scheme represents the distributions at various particle–particle separations.

gibbsite–gibbsite orientation, where the PMF profile is repulsive in pure water but becomes attractive in saline solution. In the case of gibbsite–siloxane, ions reduce the attraction slightly between the two particles. We observed the same trend for the effect of salt in the edge-to-face oriented systems, namely, that salt decreases long-range interactions between two particles. As a result, we found that in some systems, the PMF changes from repulsive to attractive due to the presence of salts. It is worth noting that in our calculations for the face-to-face orientations, the PMF profiles are limited to a minimum distance of approximately 5 Å. This is due to the fact that the free-energy barrier is very high at closer distances,[17] preventing effective sampling of the phase space[16] even though the locations of the local minima and maxima can still be identified (see Section S6 and Figure S7 of Supporting Information).

Short- and Long-Range Characteristics of PMF Profiles. The PMF profiles, as shown in Figure 2, exhibit a common feature: they are very corrugated when the interface thickness ΔZ is smaller than ca. 1.5 nm, and they are smoother for larger ΔZ. This allows us to distinguish between a short-range regime, characterized by the presence of several local minima and free-energy barriers among them in the PMF profile, and a relatively long regime.

The gibbsite–siloxane orientation shows the most intense effective attraction. In this section, we report a deeper analysis of this specific orientation. Figure 3a zooms in on the gibbsite–siloxane PMF profiles obtained with pure and saline water. In both cases, we clearly identify three local minima, the first in the case of pure water being at ΔZ = 6.2 Å, the second at 9.9 Å, and the third at 12.8 Å (as we can precisely infer from the analysis of the US simulations, see Figure S7 of Supporting Information). In almost the same position, we have the minima for saline water.[a] The main difference between the PMF profiles obtained in the pure and saline water is that the latter appears having no long-range interactions, and the intensity of the PMF minima and maxima changes slightly due to the presence of salt.

The smoothness of the long range and the corrugation of the short range can be explained in terms of the structure of the water at the interface. When the interface is thick (say, the separation between the particles is larger than ca. 1.5 nm), the water in the middle of the interface has the density of bulk liquid water at the conditions considered. See, for instance, the case of ΔZ = 2 nm in Figure 3c. In contrast, at distances shorter than 1.5 nm, the simulations show that water at the interface forms hydration layers, in a number ranging from 1 to 3. See, for instance, the case of ΔZ = 1 nm in Figure 3d, having a bilayer of water between the particles or a single layer in the case of ΔZ = 0.6 nm in Figure 3e. It shall be noticed that the presence of two or three water layers at the interface between liquid water and a solid surface is an expected feature on atomically smooth solid surfaces, observed also in experiments.[60,61] In our system, water is in fact confined in the region between the two nanoparticles, thus forming hydration layers on both the surfaces. The minima in the PMF profiles correspond to the interparticle distances that optimally accommodate 1, 2, or 3 layers, and the barriers between the minima arise because the corresponding particle–particle distances are energetically unfavorable.

The plots in Figure 3c–e show that the density of water at the interface is almost the same for pure and saline water, the latter being slightly lower due to the simultaneous presence of ions at the interface. However, at the simulated salinity, the concentration of ions is almost negligible compared to that of water, so in the plots, the density of Na^+ and Cl^- is magnified by a factor of 5. We show in Figure 3c,d the different behavior of ions at the two kaolinite faces: the gibbsite face shows a pronounced peak of Cl^- anions, and the siloxane face shows a quite smaller peak of the Na^+ cations and the absence of any Cl^- anion in its proximity. Thus, ions distribute on the two kaolinite faces to counteract the intrinsic surface charge, screening the interparticle Coulombic interaction, in agree-

https://doi.org/10.1021/acs.jpcc.2c01306
J. Phys. Chem. C XXXX, XXX, XXX–XXX

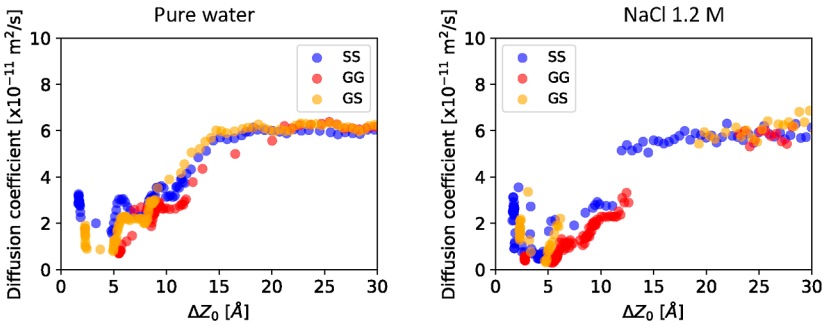

Figure 5. Diffusion coefficients along the *Z*-direction of the upper kaolinite particle in the simulation box as a function of particle−particle separation calculated for different orientations in pure water (left) and in saline water at 1.2 M NaCl concentration (right).

ment with the literature.[6,23,29] This screening effect appears as the reason for the lack of long-range interactions among the kaolinite particles in saline solution, as observed in Figure 3a.

To illustrate that the long-range attraction of the two particles is indeed due to the electrostatic interaction, we have disentangled some of the contributions that sum up to determine the overall interaction energy, and specifically the vdW and the Coulombic interparticle contributions.[b] The mean vdW and Coulombic contributions are plotted in Figure 3b as a function of the distance ΔZ. The vdW potential exhibits a short-range effect, becoming negligible beyond 1 nm. The electrostatic potential exhibits long-range features, as expected. Therefore, at distances exceeding 1 nm, the interparticle interaction is mostly due to electrostatics. We observed distinct differences in the interactions depending on the orientation of the particles. When the two approaching surfaces are dissimilar (i.e., gibbsite−siloxane), both the vdW and electrostatic potentials yield attractive interactions. In contrast, when the approaching surfaces are identical, for example, gibbsite−gibbsite and siloxane−siloxane, we observe a repulsive behavior (see Figure S8 of Supporting Information). This is due to the identical surface charges on the two approaching particles. As discussed above, in saline water, the ions deposit near the surfaces screening the long-range Coulombic attraction/repulsion.

Role of the Hydration Film. Based on the behavior of the interparticle interaction energy, see in Figure 3b, the interparticle interactions should yield smooth PMF curves. This is not the case, as observed in the previous section, and the PMF profiles exhibit a corrugated shape at distances ΔZ smaller than ca. 1.5 nm, see Figure 2. The solvent plays an important role in determining this corrugation.[17,59,62] In our study, we found that when two particles approach one another, their hydration films tend to migrate closer together and merge into a single layer at short distances. We believe that the compatibility of the two hydration films correlates with the energetic and enthalpic cost of the particle−particle aggregation.

More specifically, the aggregation of two particles at a specific orientation should be favorable if the structure of the water confined between the particles is similar to the structure of interfacial water when the particles are far away and should be unfavorable otherwise. Thus, we evaluated the distribution of the orientation of the water molecules in the first hydration layer of the bottom particle in out MD simulations. A comparison of the distributions obtained for the different orientations and at different distances, ΔZ, is reported in Figure 4. Panels (b−d) show the results of the water orientation distribution. As the two particles approach one another in the siloxane−siloxane and gibbsite−gibbsite orientations, the orientation of water molecules in the first hydration layer undergoes a significant change. In contrast, in the case of gibbsite−siloxane orientation, the distribution at various distances changes only slightly as the two particles approach each other. Similar observations are drown if we consider the one-dimensional density profiles for water hydrogen and oxygen atoms along the *Z*-direction of the simulation box for the three orientations, see Figure S10a−i and Section S9 of Supporting Information. Thus, for the gibbsite−siloxane orientation, the energy cost associated with changing the water orientation is expected to be small, different from siloxane−siloxane and gibbsite−gibbsite orientations. The above conclusion is supported also by the behavior of the solvation free energy as a function of the interparticle separation, which we have evaluated from our MD simulations and shown in Figure S9 of Supporting Information (details are in Section S8 of Supporting Information).

The hydration film has also an important effect on diffusion properties of the approaching nanoparticles. It is well known that nanoparticles in solution will exhibit a Brownian motion, with a diffusion coefficient proportional to the temperature of the system and to the inverse of the nanoparticle size, as prescribed by the Stokes−Einstein relation. Is the diffusion coefficient of a nanoparticle affected by the presence of a second nanoparticle? In which way? We evaluated the diffusion coefficient of one nanoparticle at a given distance from the other nanoparticle in our simulations using the approach of refs 63−65 and described in Section S13 of Supporting Information. Figure 5 shows the diffusion coefficients for each of the three face-to-face orientations, both for pure and saline water. At an interparticle distance ΔZ larger than 1.5 nm, the diffusion coefficient reaches a plateau of ca. 6×10^{-11} m^2/s, which appears as the bulk value of the diffusion coefficient. The bulk value appears to be the same in pure and saline water. Closer than 1.5 nm, the diffusion coefficient decreases, becoming as slow as more than six times smaller than that in the bulk. The trend of the diffusion coefficient as a function of the distance ΔZ appears only weakly affected by the specificity of the face-to-face orientation and the presence or absence of salt in water. However, it can be noticed that in saline water, the decrease in mobility is more pronounced than that in pure water.

This reduction of the nanoparticle mobility can be explained by the behavior of the hydration water. We have measured in our simulations a sharp reduction of the diffusion coefficient of water in the proximity of the nanoparticle faces, see Section

https://doi.org/10.1021/acs.jpcc.2c01306
J. Phys. Chem. C XXXX, XXX, XXX−XXX

S12 and Figure S13 of Supporting Information. Notice that this decrease in the mobility of water, and the corresponding increase in viscosity, is in good agreement with several experimental observations.[61,66] Moreover, experiments[67,68] also show that the viscosity of water increases by roughly 10% with the concentration of NaCl used in our study. The reduction of the nanoparticle mobility when closer than 1.5 nm appears to be closely related with the increased viscosity of the hydration film.

CONCLUSIONS

In this work, we have used atomistic molecular dynamics simulations and enhanced sampling techniques to investigate and characterize the interaction between two nanoparticles of kaolinite. Kaolinite particles have roughly the shape of an hexagonal prism, with the two basal faces being inequivalent, as are the side edges. As such, the interaction between two particles depends on their relative orientation. We studied the three possible face-to-face orientations and all the representative face-to-edge orientations.

A remarkable anisotropy of the interaction emerged. Face-to-edge interfaces yield a PMF that is much flatter than face-to-face interfaces. In the latter case, two of the orientations result in a repulsive interaction and one, the interface between the inequivalent faces, yields an attractive interaction. We notice that the PMF profiles exhibit different features depending on the distance between the two particle surfaces. On the one hand, by disentangling the contributions that sum up to give the overall interaction energy, we infer that the attractive or repulsive nature of the interaction, for distances larger than ca. 1.5 nm, is determined mainly by electrostatics. On the other hand, at shorter separations, the structure of water confined between the particles has to be carefully understood as this determines the interaction profile. We notice a tendency to form water layers, which correspond to the local minima in the free energy which yields a very corrugated PMF.

We have evaluated the PMF profiles in pure water and in saline solution. In saline solution, the ions have a tendency to adsorb preferentially on the basal faces of the particles, counteracting the intrinsic dipole across the kaolinite particles. Therefore, ions screen the electrostatic interparticle interaction, and the long-range PMF profiles show a much weaker interaction in saline water than that in pure water. However, ions do not appear to affect greatly the corrugation of the PMF profiles at small particle−particle separations.

Our characterization of the interaction between kaolinite nanoparticles can be compared with alternative theoretical approaches to characterize the interaction energies between (nano)-particles. The most common approach is the DLVO theory (named after Derjaguin, Landau, Verwey and Overbeek), which is in general valid at large particle−particle separations. We have here investigated the PMF profile up to 3 nm, so our approach can be complementary to DLVO as it assesses the properties of interfaces among particles at larger distances. The interval of the PMF profile that we have investigated here is, we think, the most relevant for the aggregation of particles and the formation of fines. It can be used as a solid basis for further investigations aimed at modeling the aggregation of several particles.

Experiments based on high-resolution atomic force microscopy have already provided important information on the properties of clay interfaces.[4−9] They are mostly interpreted in the context of DLVO theory and are used to estimate the surface charge distribution in clays at different environmental conditions. Hopefully, new experiments performed between isolated kaolinite particles and functionalized tips (including surface charge measurements) could validate the results presented here and provide further insights into the importance of the ionic environment on particle aggregation.

ASSOCIATED CONTENT

Supporting Information

The Supporting Information is available free of charge at https://pubs.acs.org/doi/10.1021/acs.jpcc.2c01306.

Setup of the simulations, protocol employed for enhanced sampling MD simulations and the analysis tools, validation based on comparison with *ab initio* density functional theory calculations, and some additional analysis (PDF)

AUTHOR INFORMATION

Corresponding Authors

Andrea Zen − *Dipartimento di Fisica Ettore Pancini, Università di Napoli Federico II, I-80126 Napoli, Italy; Department of Earth Sciences, University College London, London WC1E 6BT, U.K.; Thomas Young Centre and London Centre for Nanotechnology, London WC1H 0AH, U.K.*; orcid.org/0000-0002-7648-4078; Email: andrea.zen@unina.it

Angelos Michaelides − *Thomas Young Centre and London Centre for Nanotechnology, London WC1H 0AH, U.K.; Department of Physics and Astronomy, University College London, London WC1E 6BT, U.K.; Yusuf Hamied Department of Chemistry, University of Cambridge, Cambridge CB2 1EW, U.K.*; orcid.org/0000-0002-9169-169X; Email: am452@cam.ac.uk

Authors

Tai Bui − *Thomas Young Centre and London Centre for Nanotechnology, London WC1H 0AH, U.K.; BP Exploration Operating Co. Ltd, Thames TW16 7LN, U.K.; Department of Physics and Astronomy, University College London, London WC1E 6BT, U.K.*; orcid.org/0000-0002-0692-5229

Tran Thi Bao Le − *Department of Chemical Engineering, University College London, WC1E 7JE London, U.K.*

Weparn J. Tay − *BP Exploration Operating Co. Ltd, Thames TW16 7LN, U.K.*

Kuhan Chellappah − *BP Exploration Operating Co. Ltd, Thames TW16 7LN, U.K.*; orcid.org/0000-0001-9947-8087

Ian R. Collins − *BP Exploration Operating Co. Ltd, Thames TW16 7LN, U.K.*

Richard D. Rickman − *BP Exploration Operating Co. Ltd, Thames TW16 7LN, U.K.*

Alberto Striolo − *Department of Chemical Engineering, University College London, WC1E 7JE London, U.K.; School of Chemical, Biological and Materials Engineering, University of Oklahoma, Norman, Oklahoma 73019, United States*; orcid.org/0000-0001-6542-8065

Complete contact information is available at: https://pubs.acs.org/10.1021/acs.jpcc.2c01306

Author Contributions

○A.Z. and T.B. contributed equally

Notes

The authors declare no competing financial interest.

■ ACKNOWLEDGMENTS

We thank Stephen J. Cox and Andrey G. Kalinichev for insightful discussions. A.Z. acknowledges financial support from the Leverhulme Trust, grant number RPG-2020-038. This work was also supported by the BP Exploration Operating Company Limited, University College London/The Thomas Young Centre, and Innovative UK under the Knowledge Transfer Partnership, grant number KTP011009. We are also grateful, for computational resources, to the BP HPC facilities, to ARCHER UK National Supercomputing Service, the United Kingdom Car Parrinello (UKCP) consortium (EP/F036884/1), the London Centre for Nanotechnology and University College London Research Computing, the UCL Myriad and Kathleen High Performance Computing Facility (Myriad@UCL, Kathleen@UCL), the U.K. Materials and Molecular Modelling Hub for computational resources, which is partially funded by EPSRC (EP/P020194/1 and EP/T022213/1), the CPU hours by CSCS under project ID s1000, the Cambridge Service for Data Driven Discovery (CSD3) operated by the University of Cambridge Research Computing Service (www.csd3.cam.ac.uk), provided by Dell EMC and Intel using Tier-2 funding from the Engineering and Physical Sciences Research Council (capital grant EP/P020259/1), and DiRAC funding from the Science and Technology Facilities Council (www.dirac.ac.uk).

■ ADDITIONAL NOTES

[a]Notice that this almost exact match of the minima locations for the pure and saline water solution is observed in most the PMF profiles studied there.

[b]In this contribution, we are just considering the two particles and ignoring anything else (water and ions).

■ REFERENCES

(1) *Handbook of Clay Science*, 1st ed.; Bergaya, F., Theng, B., Lagaly, G., Eds.; Elsevier, 2006.

(2) Lagaly, G. Handbook of Clay Science. In *Developments in Clay Science*; Bergaya, F., Theng, B. K., Lagaly, G., Eds.; Elsevier, 2006; Vol. *1*; pp 141−245.

(3) Brigatti, M. F.; Galan, E.; Theng, B. K. G. Handbook of Clay Science. In *Developments in Clay Science*; Bergaya, F., Theng, B. K., Lagaly, G., Eds.; Elsevier, 2006; Vol. *1*; pp 19−86.

(4) Siretanu, I.; Ebeling, D.; Andersson, M. P.; Stipp, S. L.; Philipse, A.; Stuart, M. C.; Van Den Ende, D.; Mugele, F. Direct observation of ionic structure at solid-liquid interfaces: A deep look into the Stern Layer. *Sci. Rep.* **2014**, *4*, 19−21.

(5) Kumar, N.; Zhao, C.; Klaassen, A.; Van den Ende, D.; Mugele, F.; Siretanu, I. Characterization of the surface charge distribution on kaolinite particles using high resolution atomic force microscopy. *Geochim. Cosmochim. Acta* **2016**, *175*, 100−112.

(6) Kumar, N.; Andersson, M. P.; Van Den Ende, D.; Mugele, F.; Siretanu, I. Probing the Surface Charge on the Basal Planes of Kaolinite Particles with High-Resolution Atomic Force Microscopy. *Langmuir* **2017**, *33*, 14226−14237.

(7) Gupta, V.; Miller, J. D. Surface force measurements at the basal planes of ordered kaolinite particles. *J. Colloid Interface Sci.* **2010**, *344*, 362−371.

(8) Gupta, V.; Hampton, M. A.; Stokes, J. R.; Nguyen, A. V.; Miller, J. D. Particle interactions in kaolinite suspensions and corresponding aggregate structures. *J. Colloid Interface Sci.* **2011**, *359*, 95−103.

(9) Liu, J.; Sandaklie-Nikolova, L.; Wang, X.; Miller, J. D. Surface force measurements at kaolinite edge surfaces using atomic force microscopy. *J. Colloid Interface Sci.* **2014**, *420*, 35−40.

(10) Dishon, M.; Zohar, O.; Sivan, U. From repulsion to attraction and back to repulsion: The effect of NaCl, KCl, and CsCl on the force between silica surfaces in aqueous solution. *Langmuir* **2009**, *25*, 2831−2836.

(11) Tombácz, E.; Szekeres, M. Surface charge heterogeneity of kaolinite in aqueous suspension in comparison with montmorillonite. *Appl. Clay Sci.* **2006**, *34*, 105−124.

(12) Gan, Y.; Franks, G. V. Charging behavior of the gibbsite basal (001) surface in NaCl solution investigated by AFM colloidal probe technique. *Langmuir* **2006**, *22*, 6087−6092.

(13) Hu, J.; Xiao, X.-D.; Ogletree, D. F.; Salmeron, M. Imaging the condensation and evaporation of molecularly thin films of water with nanometer resolution. *Science* **1995**, *268*, 267−269.

(14) Furukawa, Y.; Watkins, J. L.; Kim, J.; Curry, K. J.; Bennett, R. H. Aggregation of montmorillonite and organic matter in aqueous media containing artificial seawater. *Geochem. Trans.* **2009**, *10*, 1−11.

(15) Volkova, E.; Nair, A. K. N.; Engelbrecht, J.; Schwingenschlögl, U.; Sun, S.; Stenchikov, G. Molecular Dynamics Modeling of Kaolinite Particle Associations. *J. Phys. Chem. C* **2021**, *125*, 24126−24136.

(16) Shen, X.; Bourg, I. C. Molecular dynamics simulations of the colloidal interaction between smectite clay nanoparticles in liquid water. *J. Colloid Interface Sci.* **2021**, *584*, 610−621.

(17) Ho, T. A.; Criscenti, L. J. Molecular-level understanding of gibbsite particle aggregation in water. *J. Colloid Interface Sci.* **2021**, *600*, 310−317.

(18) Ebrahimi, D.; Pellenq, R. J.-M.; Whittle, A. J. Nanoscale elastic properties of montmorillonite upon water adsorption. *Langmuir* **2012**, *28*, 16855−16863.

(19) Ebrahimi, D.; Whittle, A. J.; Pellenq, R. J.-M. Mesoscale properties of clay aggregates from potential of mean force representation of interactions between nanoplatelets. *J. Chem. Phys.* **2014**, *140*, 154309.

(20) Ebrahimi, D.; Pellenq, R. J.-M.; Whittle, A. J. Mesoscale simulation of clay aggregate formation and mechanical properties. *Granul. Matter* **2016**, *18*, 49.

(21) Liu, X.; Lu, X.; Meijer, E. J.; Wang, R.; Zhou, H. Atomic-scale structures of interfaces between phyllosilicate edges and water. *Geochim. Cosmochim. Acta* **2012**, *81*, 56−68.

(22) Liu, J.; Lin, C.-L.; Miller, J. D. Simulation of cluster formation from kaolinite suspensions. *Int. J. Miner. Process.* **2015**, *145*, 38−47.

(23) Vasconcelos, I. F.; Bunker, B. A.; Cygan, R. T. Molecular dynamics modeling of ion adsorption to the basal surfaces of kaolinite. *J. Phys. Chem. C* **2007**, *111*, 6753−6762.

(24) Li, X.; Li, H.; Yang, G. Promoting the adsorption of metal ions on kaolinite by defect sites: A molecular dynamics study. *Sci. Rep.* **2015**, *5*, 28−30.

(25) Li, X.; Li, H.; Yang, G. Configuration, anion-specific effects, diffusion, and impact on counterions for adsorption of salt anions at the interfaces of clay minerals. *J. Phys. Chem. C* **2016**, *120*, 14621−14630.

(26) Zhang, L.; Lu, X.; Liu, X.; Yang, K.; Zhou, H. Surface Wettability of Basal Surfaces of Clay Minerals: Insights from Molecular Dynamics Simulation. *Energy Fuel.* **2016**, *30*, 149−160.

(27) Underwood, T.; Erastova, V.; Greenwell, H. C. Wetting Effects and Molecular Adsorption at Hydrated Kaolinite Clay Mineral Surfaces. *J. Phys. Chem. C* **2016**, *120*, 11433−11449.

(28) Underwood, T. R.; Bourg, I. C. Large-Scale Molecular Dynamics Simulation of the Dehydration of a Suspension of Smectite Clay Nanoparticles. *J. Phys. Chem. C* **2020**, *124*, 3702−3714.

(29) Papavasileiou, K. D.; Michalis, V. K.; Peristeras, L. D.; Vasileiadis, M.; Striolo, A.; Economou, I. G. Molecular Dynamics Simulation of Water-Based Fracturing Fluids in Kaolinite Slit Pores. *J. Phys. Chem. C* **2018**, *122*, 17170−17183.

(30) Sayer, T.; Cox, S. J. Macroscopic surface charges from microscopic simulations. *J. Chem. Phys.* **2020**, *153*, 164709.

https://doi.org/10.1021/acs.jpcc.2c01306
J. Phys. Chem. C XXXX, XXX, XXX−XXX

(31) Tazi, S.; Rotenberg, B.; Salanne, M.; Sprik, M.; Sulpizi, M. Absolute acidity of clay edge sites from ab-initio simulations. *Geochim. Cosmochim. Acta* **2012**, *94*, 1−11.
(32) Liu, X.; Lu, X.; Sprik, M.; Cheng, J.; Meijer, E. J.; Wang, R. Acidity of edge surface sites of montmorillonite and kaolinite. *Geochim. Cosmochim. Acta* **2013**, *117*, 180−190.
(33) Liu, X.; Cheng, J.; Sprik, M.; Lu, X.; Wang, R. Surface acidity of 2:1-type dioctahedral clay minerals from first principles molecular dynamics simulations. *Geochim. Cosmochim. Acta* **2014**, *140*, 410−417.
(34) Hu, X. L.; Michaelides, A. Water on the hydroxylated (0 0 1) surface of kaolinite: From monomer adsorption to a flat 2D wetting layer. *Surf. Sci.* **2008**, *602*, 960−974.
(35) Presti, D.; Pedone, A.; Mancini, G.; Duce, C.; Tiné, M. R.; Barone, V. Insights into structural and dynamical features of water at halloysite interfaces probed by DFT and classical molecular dynamics simulations. *Phys. Chem. Chem. Phys.* **2016**, *18*, 2164−2174.
(36) Liao, B.; Qiu, L.; Wang, D.; Bao, W.; Wei, Y.; Wang, Y. The behaviour of water on the surface of kaolinite with an oscillating electric field. *RSC Adv.* **2019**, *9*, 21793−21803.
(37) Pouvreau, M.; Greathouse, J. A.; Cygan, R. T.; Kalinichev, A. G. Structure of Hydrated Kaolinite Edge Surfaces: DFT Results and Further Development of the ClayFF Classical Force Field with Metal-O-H Angle Bending Terms. *J. Phys. Chem. C* **2019**, *123*, 11628−11638.
(38) Kameda, J.; Yamagishi, A.; Kogure, T. Morphological characteristics of ordered kaolinite: Investigation using electron back-scattered diffraction. *Am. Mineral.* **2005**, *90*, 1462−1465.
(39) Bish, D. L. Rietveld refinement of the kaolinite structure at 1.5 K. *Clays Clay Miner.* **1993**, *41*, 738−744.
(40) Plimpton, S. Fast Parallel Algorithms for Short-Range Molecular Dynamics. *J. Comput. Phys.* **1995**, *117*, 1−19.
(41) Cygan, R. T.; Liang, J.-J.; Kalinichev, A. G. Molecular models of hydroxide, oxyhydroxide, and clay phases and the development of a general force field. *J. Phys. Chem. B* **2004**, *108*, 1255−1266.
(42) Pouvreau, M.; Greathouse, J. A.; Cygan, R. T.; Kalinichev, A. G. Structure of Hydrated Gibbsite and Brucite Edge Surfaces: DFT Results and Further Development of the ClayFF Classical Force Field with Metal-O-H Angle Bending Terms. *J. Phys. Chem. C* **2017**, *121*, 14757−14771.
(43) Cygan, R. T.; Greathouse, J. A.; Kalinichev, A. G. Advances in Clayff Molecular Simulation of Layered and Nanoporous Materials and Their Aqueous Interfaces. *J. Phys. Chem. C* **2021**, *125*, 17573−17589.
(44) Berendsen, H. J. C.; Grigera, J. R.; Straatsma, T. P. The missing term in effective pair potentials. *J. Phys. Chem.* **1987**, *91*, 6269−6271.
(45) Smith, D. E.; Dang, L. X. Computer simulations of NaCl association in polarizable water. *J. Chem. Phys.* **1994**, *100*, 3757−3766.
(46) Ryckaert, J.-P.; Ciccotti, G.; Berendsen, H. J. C. Numerical integration of the cartesian equations of motion of a system with constraints: molecular dynamics of n-alkanes. *J. Comput. Phys.* **1977**, *23*, 327−341.
(47) Ho, T. A.; Greathouse, J. A.; Wang, Y.; Criscenti, L. J. Atomistic Structure of Mineral Nano-aggregates from Simulated Compaction and Dewatering. *Sci. Rep.* **2017**, *7*, 15286.
(48) Ho, T. A.; Greathouse, J. A.; Lee, A. S.; Criscenti, L. J. Enhanced Ion Adsorption on Mineral Nanoparticles. *Langmuir* **2018**, *34*, 5926−5934.
(49) Hockney, R. W.; Eastwood, J. W. *Computer simulation using particles*; crc Press: Bristol: Hilger, 1988.
(50) Zen, A.; Roch, L. M.; Cox, S. J.; Hu, X. L.; Sorella, S.; Alfè, D.; Michaelides, A. Toward accurate adsorption energetics on clay surfaces. *J. Phys. Chem. C* **2016**, *120*, 26402−26413.
(51) Nosé, S. A unified formulation of the constant temperature molecular dynamics methods. *J. Chem. Phys.* **1984**, *81*, 511−519.
(52) Torrie, G. M.; Valleau, J. P. Monte Carlo free energy estimates using non-Boltzmann sampling: Application to the sub-critical Lennard-Jones fluid. *Chem. Phys. Lett.* **1974**, *28*, 578−581.
(53) Torrie, G. M.; Valleau, J. P. Nonphysical sampling distributions in Monte Carlo free-energy estimation: Umbrella sampling. *J. Comput. Phys.* **1977**, *23*, 187−199.
(54) Fiorin, G.; Klein, M. L.; Hénin, J. Using collective variables to drive molecular dynamics simulations. *Mol. Phys.* **2013**, *111*, 3345−3362.
(55) White, G. N. Analysis and Implications of the Edge Structure of Dioctahedral Phyllosilicates. *Clays Clay Miner.* **1988**, *36*, 141−146.
(56) Hu, X. L.; Michaelides, A. The kaolinite (0 0 1) polar basal plane. *Surf. Sci.* **2010**, *604*, 111−117.
(57) Argyris, D.; Cole, D. R.; Striolo, A. Hydration Structure on Crystalline Silica Substrates. *Langmuir* **2009**, *25*, 8025−8035.
(58) Fan, H.; Resasco, D. E.; Striolo, A. Amphiphilic Silica Nanoparticles at the Decane-Water Interface: Insights from Atomistic Simulations. *Langmuir* **2011**, *27*, 5264−5274.
(59) Argyris, D.; Phan, A.; Striolo, A.; Ashby, P. D. Hydration structure at the α-Al2O3 (0001) surface: Insights from experimental atomic force spectroscopic data and atomistic molecular dynamics simulations. *J. Phys. Chem. C* **2013**, *117*, 10433−10444.
(60) Björneholm, O.; Hansen, M. H.; Hodgson, A.; Liu, L.-M.; Limmer, D. T.; Michaelides, A.; Pedevilla, P.; Rossmeisl, J.; Shen, H.; Tocci, G.; Tyrode, E.; Walz, M.-M.; Werner, J.; Bluhm, H. Water at Interfaces. *Chem. Rev.* **2016**, *116*, 7698−7726.
(61) Raviv, U.; Perkin, S.; Laurat, P.; Klein, J. Fluidity of Water Confined Down to Subnanometer Films. *Langmuir* **2004**, *20*, 5322−5332.
(62) van Lin, S. R.; Grotz, K. K.; Siretanu, I.; Schwierz, N.; Mugele, F. Ion-Specific and pH-Dependent Hydration of Mica−Electrolyte Interfaces. *Langmuir* **2019**, *35*, 5737−5745.
(63) Woolf, T. B.; Roux, B. Conformational Flexibility of o-Phosphorylcholine and o-Phosphorylethanolamine: A Molecular Dynamics Study Solvation Effects. *J. Am. Chem. Soc.* **1994**, *116*, 5916−5926.
(64) Hummer, G. Position-dependent diffusion coefficients and free energies from Bayesian analysis of equilibrium and replica molecular dynamics simulations. *New J. Phys.* **2005**, *7*, 34.
(65) Phan, A.; Bui, T.; Acosta, E.; Krishnamurthy, P.; Striolo, A. Molecular mechanisms responsible for hydrate anti-agglomerant performance. *Phys. Chem. Chem. Phys.* **2016**, *18*, 24859−24871.
(66) Raviv, U.; Laurat, P.; Klein, J. Fluidity of water confined to subnanometre films. *Nature* **2001**, *413*, 51−54.
(67) Phillips, S.; Ozbek, H.; Igbene, A.; Litton, G. *Viscosity of NaCl and Other solutions up to 350 °C and 50 MPa Pressures*; Lawrence Berkeley National Laboratory, 1980.
(68) Kestin, J.; Khalifa, H. E.; Correia, R. J. Tables of the dynamic and kinematic viscosity of aqueous NaCl solutions in the temperature range 20−150 °C and the pressure range 0.1−35 MPa. *J. Phys. Chem. Ref. Data* **1981**, *10*, 71−88.

https://doi.org/10.1021/acs.jpcc.2c01306
J. Phys. Chem. C XXXX, XXX, XXX−XXX